scientific reports

Check for updates

OPEN

Crystal structure of Au-pseudocarbyne(C_6)

Jun Wu[1,2]✉, Pilarisetty Tarakeshwar[1], Scott G. Sayres[1,3], Moreno Meneghetti[4], Hyunsub Kim[1,3], Juan Barreto[1] & Peter R. Buseck[1,2]✉

Carbyne-related materials permit exploring the potentially extraordinary properties of this long-sought but still elusive carbon allotrope. However, accurate understanding of these materials is challenging. Here we report the crystal structure of a Au-pseudocarbyne, a representative of a possible new family of materials consisting of *sp*-hybridized carbon chains and stabilizing metal atoms. Au-pseudocarbyne(C_6), the representative pseudocarbyne containing six-membered carbon chains, has space group P6/mmm[191] and unit-cell parameters $a = b = 0.60$ nm, $c = 0.896$ nm, $\alpha = \beta = 90°$, $\gamma = 120°$. Its long-range structure can be understood as intimately intergrown bundles, each consisting of six parallel, infinite carbon chains surrounding a column of gold atoms. This compound, together with its eight-membered counterpart Au-pseudocarbyne(C_8), shows that interesting new materials resembling the carbyne structure and sharing some of its properties can be designed and developed. The current work raises serious questions regarding recent reports of carbyne synthesis.

Keywords Pseudocarbyne, Carbyne, *sp* hybridization, Linear carbon chains, Gold-carbon bond

Carbon allotropes containing sp^2 and sp^3 hybridization are well known and have collectively enabled a wide range of new science and technological applications. Carbyne, the controversial *sp*-hybridized allotrope, is a notable exception. Recent reports of the synthesis and characterization of pseudocarbynes, plausibly related materials that contain *sp*-hybridized carbon chains plus gold[1–3], provide the motivation for exploring their structures and possible relation to carbyne.

Carbyne existence has been a contentious topic and several portrayals of its purported structure exist[4–7]. In the condensed phase, carbyne is considered the one-dimensional infinite carbon polymer with either alternating C-C (single) and C≡C (triple) bonds (polyynes) or a continuous strand of C=C double bonds (cumulenes). Although single carbon chains in solution have been experimentally isolated and characterized[8,9], attempts to isolate them as solids[10–17] are unsubstantiated. The unpaired electrons on either end of the chains make the carbon atoms in the chain highly reactive and lead to rapid crosslinking and explosive polymerization[18,19]. To overcome this extreme reactivity, extensive efforts have been made to end-cap the carbon chains with organic functional groups or metal complexes[20,21]. Such interchain stabilization may have been overlooked in subsequent studies, raising the question of whether the claimed carbynes in numerous reports[22–29] are real or materials masquerading as carbyne.

Stimulated by and skeptical of reported synthesis of crystalline carbyne in the presence of gold[30], and based on theoretical calculations, we hypothesized the existence of a new chemical system that we called pseudocarbyne[1]. It is characterized by *sp*-hybridized carbon chains stabilized by charge-dissipating groups such as metal atoms, clusters, or complexes between the chains. The configuration and compactness of the chains in pseudocarbyne differ from polyynes end-capped with large metal–organic complexes[21,31]. Recently, Salazar et al. produced pseudocarbynes stabilized by gold thiolates[32].

Pseudocarbyne structures depend on the lengths of their carbon chains as well as on extraneous atoms or atom groups. The current study considers Au-pseudocarbynes with chains containing six and eight carbons, which we call Au-pseudocarbyne(C_6) and Au-pseudocarbyne(C_8), respectively. Experimental spectroscopic, x-ray, and electron-microscopy measurements are combined with theoretical data to determine the crystal structure of Au-pseudocarbyne(C_6) in particular. In the process, evidence has been generated that suggests a family of related pseudocarbyne species. We propose that they form a homologous series with -C≡C– as the repeating unit.

[1]School of Molecular Sciences, Arizona State University, Tempe, AZ 85287, USA. [2]School of Earth and Space Exploration, Arizona State University, Tempe, AZ 85287, USA. [3]Biodesign Center for Applied Structural Discovery, Arizona State University, Tempe, AZ 85287, USA. [4]Department of Chemical Sciences, University of Padova, 35131 Padova, Italy. ✉email: junwu1@asu.edu; pbuseck@asu.edu

Methods

Materials

Samples were prepared using either laser ablation in liquid (LAL) with gold targets[2] or self-assembly of carbon chains produced by prompt mixing of solutions containing polyynes and gold nanoparticles[3]. Both methods produced microgram quantities of products. The products were identified and confirmed using ultraviolet–visible (UV–vis) absorption, Fourier-transform infrared (FTIR), and micro-Raman spectra[2,3].

Powder x-ray diffraction (PXRD)

PXRD measurements were made with Cu *K*α radiation (λ = 0.15406 nm). The data were processed using standard background subtraction and subsequent peak offset by reference to the peak positions of gold, which occurs as a minor impurity in all our samples and thus can serve as an internal standard.

Electron microscopy and related spectroscopy

Transmission electron microscopy (TEM) was done using several instruments. Conventional TEM images and selected-area electron diffraction (SAED) patterns were acquired using a Philips CM200 electron microscope with a field-emission gun, operated at a 200-kV accelerating voltage. Chemical measurements were made with an Oxford x-ray energy-dispersive spectroscopy (EDS) detector attached to the microscope. High-resolution scanning transmission electron microscopy (STEM) and high-angle annular dark field (HAADF) images were obtained using a JEOL ARM200F aberration-corrected microscope equipped with a Schottky field-emission gun, operated at 200 kV to permit imaging resolutions of 0.19 nm and 0.08 nm in TEM and STEM mode, respectively. Electron energy-loss spectroscopy (EELS) maps were obtained using an aberration-corrected FEI Titan microscope operated at 300 kV and equipped with a gun monochromator to achieve 0.1-eV energy resolution. The electron voltages used in the current work are the same as those in the claimed carbyne report where only the unit-cell parameters were determined for materials synthesized using a similar method[30]. For compositional mapping, we used copper grids coated with thin films of amorphous silicon monoxide to avoid carbon signals from standard TEM grids. Prior to use, the grids were cooled to liquid-nitrogen temperature using a Gatan CT3500 cryo holder to minimize radiation damage.

Structure determination

Spectroscopic investigations made using Raman, FTIR, UV–vis, EDS and EELS methods indicate that the pseudocarbyne materials possess both C≡C triple bonds and gold. Adding information from PXRD, SAED, TEM, and STEM measurements enabled determination of the unit-cell geometry, locations of gold atoms, and placement of carbon chains. We optimized gold-carbon distances and chain zigzags to position the carbon atoms within the unit cell by using the PXRD peak intensity ratios.

Experimental results

Our prior spectroscopic measurements display distinctive features[2,3]. Raman spectra of several samples have strong peaks at ~ 2178 and ~ 316 cm^{-1}, and a few samples also exhibit weak peaks at 1050 cm^{-1}. On the other hand, FTIR spectra have a strong peak at 2157 cm^{-1}, and UV spectra show strong absorption peaks at 205, 212, 218, and 231 nm.

Compositional analyses using EDS in the electron microscope indicate that the samples consist of carbon with a few molar percent of gold. EELS signals near the C-*K* and Au-$M_{4,5}$ edges, respectively, provide rough maps of the carbon and gold distribution that are consistent with the corresponding HAADF image (Fig. 1). Subtracting the substrate silicon and background signals from the spectrum produced the gold signal. The region between 2250 and 2880 eV, within the vertical dashed lines, was then used to generate the gold map.

The relatively poor signal-to-noise ratio for gold results from its low concentration and superimposed Si-*K* edge. The resultant maps indicate a uniform distribution of both carbon and gold at a spatial scale of 2.4×2.4 nm^2 in the samples upon initial imaging (Fig. 1). As discussed in the section titled Structural gold below, the gold distribution becomes non-uniform upon exposure to the electron beam.

Major peaks for *d*-spacings of 0.896, 0.448, 0.299, and 0.224 nm occur in all PXRD patterns[3]. Small pre-peaks indicate slightly greater *d*-spacings, implying that materials with longer carbon chains are also produced but in much lower amounts. The pre-peak intensities decrease with aging, indicating the relative instability of structures with long chains. The ratio of normalized intensities between the major peaks in the PXRD patterns show significant variations among samples, with the smallest ratio of 0.27 measured for the first two major peaks.

Most gold pseudocarbyne grains in our samples assume platy morphologies, have > 1-μm diameters, and 30- to 100-nm thicknesses. Their SAED patterns and TEM images indicate hexagonal or trigonal symmetry (Fig. 2a,b). In a few places, the platy grains occur in edge-on orientations so that lattice fringes with *d*-spacings between ~ 0.87 and ~ 0.93 nm are evident (Fig. 2c,d). As explained in the Structural gold section, the dark spots ~ 5 nm across in Fig. 2a,c are produced by gold nanoparticles generated during electron irradiation. They were avoided during imaging.

Elongated grains with spindle- or needle-like shapes are much less common. Their lengths range from one tenth to a few micrometers (Fig. 3a). The grains consist of fibrous nanodomains that are oriented roughly parallel to the grain lengths, are a few nanometers wide, up to a hundred nanometers long, and display ~ 1.02-nm lattice fringes perpendicular to the nanodomain lengths (Figs. 3b,d). When viewed end-on, the nanodomains are roughly equidimensional with small gaps between some of them. The symmetry and geometry of their spot patterns revealed in STEM mode are identical to those of the platy crystals in TEM (Fig. 3c).

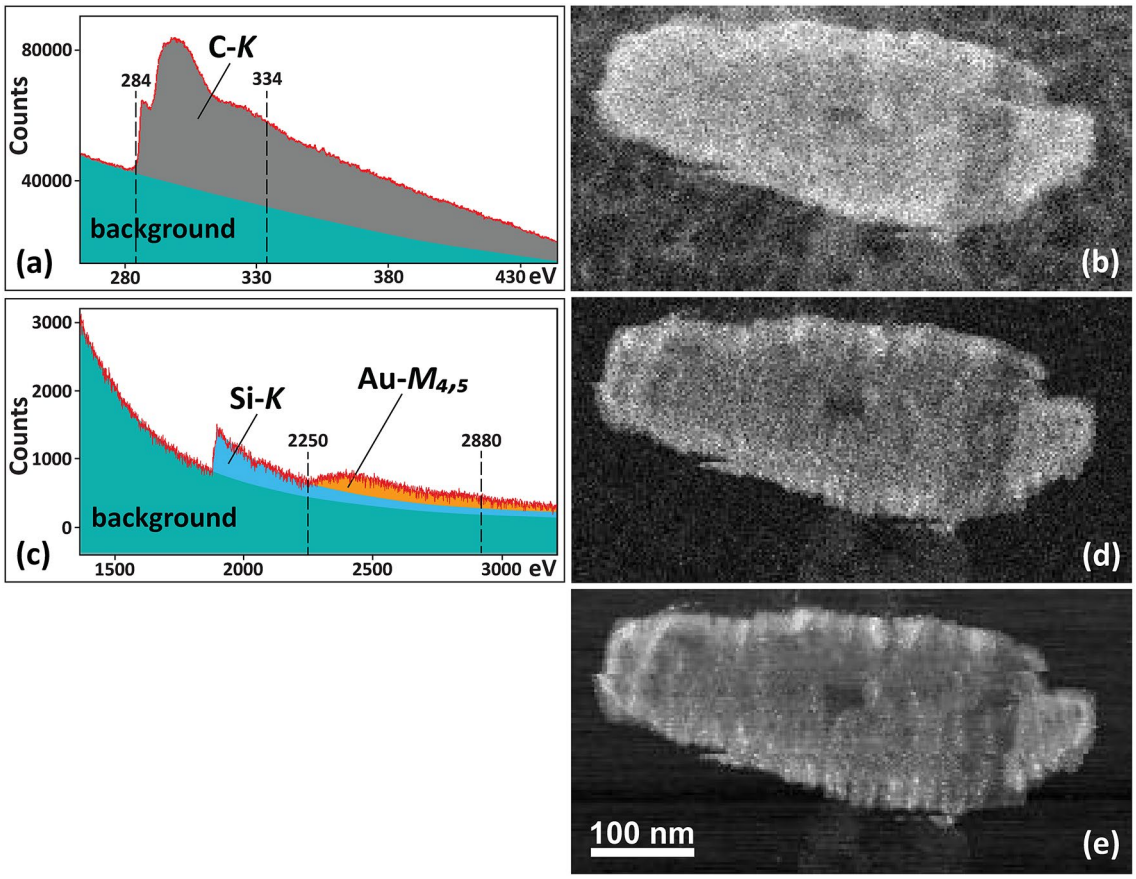

Fig. 1. Composition of a gold pseudocarbyne grain. (**a**) Composite core-loss EELS spectrum (red) of signals from the sample's carbon *K* edge (gray) and background (turquoise). (**b**) Carbon map generated using the signal between 284 and 334 eV. The uniform intensity indicates a relatively even thickness. (**c**) Composite core-loss EELS spectrum (red) of signals from the sample's gold $M_{4,5}$ edges (orange), silicon *K* edge from the SiO supporting substrate (blue), and background (turquoise), collected within a higher energy range than that in (**a**). (**d**) Gold map. The bright spots concentrated along the grain edges result from gold nanoparticles. Except at the edges, a fairly uniform gold signal occurs throughout the grain. (**e**) HAADF image of the same grain upon initial electron-beam exposure shows prominent bright spots near its edges, at the same positions as in (**d**).

Interpretation and discussion

Structural gold

The evidence for gold within the pseudocarbyne structure is compelling. EDS analyses indicate that the samples contain a small concentration of gold. STEM-EELS maps indicate a uniform gold distribution within relatively fresh sample areas. Gold nanoparticle growth, structural continuity between these nanoparticles and the matrix, and contrast in STEM images are all consistent with the occurrence of structural gold.

When samples are first exposed to an electron beam, gold nanoparticles appear (see SI). They are uniformly distributed and roughly round with ~ 1-nm diameters. Upon continued exposure to the beam, the nanoparticles increase in number and size until they approach ~ 10 nm across. At that point growth stops, although electron-induced particle coalescence occurs. These results indicate that gold in these nanoparticles is locally sourced during their growth, consistent with starting materials in which carbon and gold are the only non-volatile elements. Similar growth of gold nanoparticles occurs when pseudocarbynes are heated. We interpret the size increases of the gold nanoparticles within pseudocarbynes as resulting from gold release from within the structure.

Coherent or semi-coherent boundaries in two dimensions occur between gold nanoparticles and the parent pseudocarbyne. This structural continuity between the two types of material explains why gold is so readily released from the pseudocarbyne grains upon irradiation, analogous to the development of iron nanoparticles from $La_{0.6}Sr_{0.4}FeO_3$ perovskite in which a coherent interface forms between the new phase and host structure[33].

High-resolution STEM-HAADF images of pseudocarbyne show regularly spaced bright spots. Unlike in TEM images, the spots in these STEM images indicate the actual positions of atomic columns. The pronounced contrast between these spots and the surrounding regions indicates that the atoms in the columns have a high atomic number and are embedded within a matrix of atoms having a low atomic number. Also, the similar contrast between the periodically arranged bright spots and the irradiation-released gold nanoparticles indicates

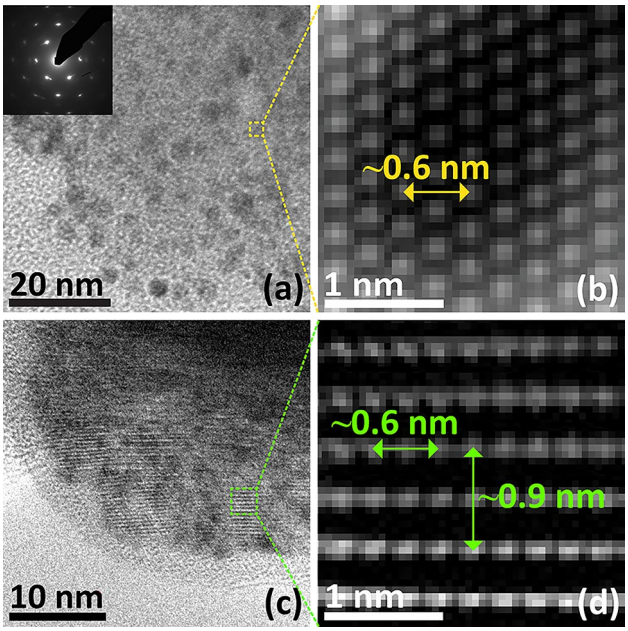

Fig. 2. TEM images of platy pseudocarbyne. (**a**) Platy crystal and its SAED pattern. (**b**) Enlargement of the filtered Fourier image of the area in the yellow dashed square. (**c**) Edge-on view of a platy crystal showing the ~ 0.9-nm lattice fringes. (**d**) Enlargement of the filtered Fourier image of the area in the green dashed square.

that these bright spots correspond to atoms having a mean atomic number consistent with that of gold. Thus, the evidence is overwhelming that the bright spots arise from gold in a matrix of carbon.

Spectroscopy

The strong Raman peak at ~ 2178 cm^{-1} arises from a C≡C stretch that is characteristic of *sp* carbon and confirms that the samples only contain C≡C bonds[2,3]. The absence of Raman peaks in the 1400–1800 cm^{-1} region precludes the occurrence of species containing C=C double bonds.

Bare polyynes do not exhibit Raman bending modes below ~ 500 cm^{-1}. The strong Raman peak observed at around ~ 316 cm^{-1} indicates that the sample is associated with a metallic species, which in our case is gold. Our prior work shows that the existence and intensity of the weak ~ 1050 cm^{-1} peak, which arises from a C–C single bond stretch, depend on the proximity of foreign gold clusters or atoms[1,2]. These gold entities occur at various distances from the C–C single bonds in different pseudocarbynes, thereby explaining the variations in intensity of this Raman peak.

The occurrence of an IR peak at ~ 2157 cm^{-1} suggests that gold atoms are influencing the C≡C stretching frequencies. We interpret the combination of the Raman and FTIR results as compelling evidence of a pseudocarbyne[2,3].

The UV absorption spectra of our samples arise from the $1\Sigma_u^+ \leftarrow 1\Sigma_g^+$ transition of systems containing C≡C bonds[2,34]. The UV peaks are distinct from absorbances known for gold nanoparticles or ligand-passivated gold nanoclusters. Comparison with the UV spectra of systems containing C≡C bonds such as bare polyynes indicates that the carbon chains in our samples contain a finite number of carbon atoms[2,34].

As described in our previous work, several products belonging to the pseudocarbyne family are likely produced through the synthetic processes[1,2]. The current report provides new TEM results about two crystalline products that contain gold atoms. Other pseudocarbyne products that are suspected to occur within the liquid samples would presumably provide contributions to the macroscopic spectroscopic measurements, but these are not characterized by TEM in the current work.

Unit-cell geometry

Determination of the unit-cell geometry is based on PXRD, TEM, and STEM measurements. High-resolution TEM and STEM images plus SAED patterns show hexagonal or trigonal symmetry, consistent with our observation that large spacings occur only in one direction in any given pseudocarbyne grain. Further considerations of space group and symmetry elements eliminate the possibility of trigonal symmetry.

The positions of the relatively narrow, high-intensity PXRD peaks suggest that they are a harmonic series of *00l* reflections. The absence of glide planes and screw axes in the structure, which is necessitated by the chemical constraints of the high carbon concentration, indicates that the first strong peak is from (001) planes. This peak assignment reflects the strong preferred orientation seen in TEM for the platy grains, where the largest lattice-fringe spacing matches that of the first major PXRD peak. Variations in relative intensities of *001* to higher-order *00l* peaks in different samples result from overlapping peaks from other planes in the structure, *e.g.*, {101}, plus minor differences in the extent of preferred orientation.

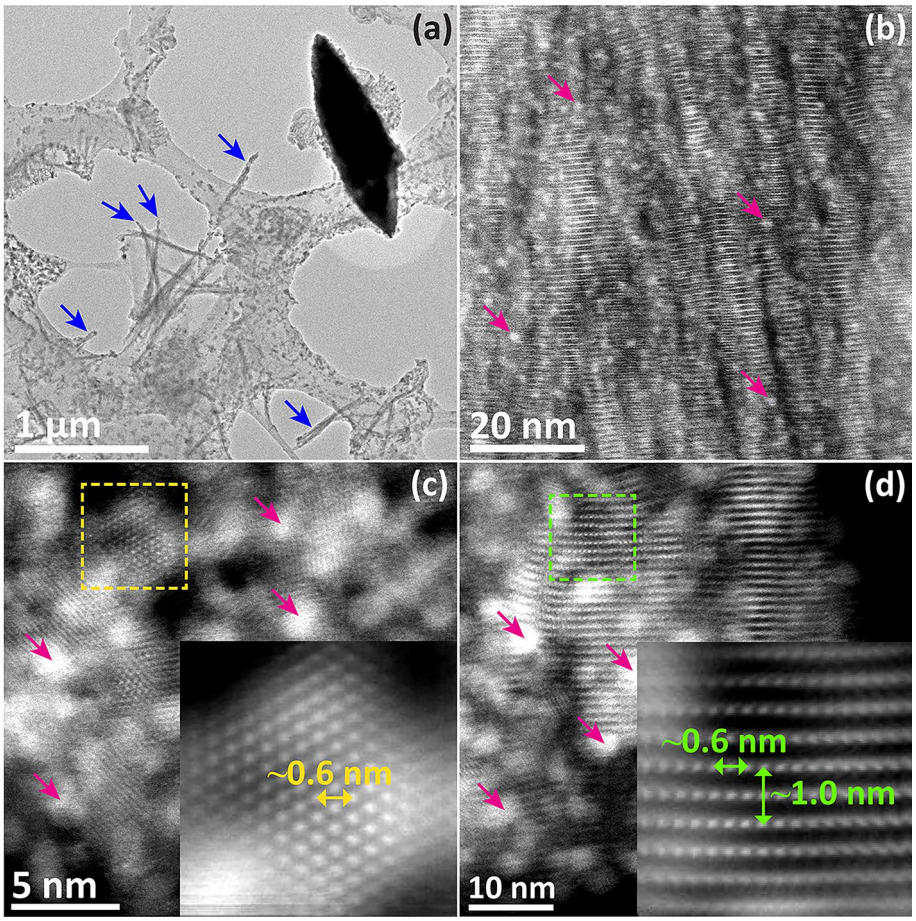

Fig. 3. TEM and STEM images of elongated pseudocarbyne crystals. The prominent white spots with fuzzy edges and diameters of several nanometers in the STEM images (*e.g.*, magenta arrows) are gold nanoparticles and were avoided for imaging. (**a**) TEM image of a large spindle- and multiple needle-shaped crystals (*e.g.*, blue arrows). (**b**) HAADF image of the thin area of a spindle viewed perpendicular to its length. (**c**) HAADF image of the cross section of a spindle. The inset shows an enlargement of the filtered Fourier image of the area in the yellow dashed square. (**d**) HAADF image of a crystal similar to that in (**c**) but with the same orientation as in (**b**). The inset shows an enlargement of the filtered Fourier image of the area in the green dashed square.

Crystal planes with ~ 1.02-nm *d*-spacings occur in TEM images of elongated grains and produce a small pre-peak in PXRD patterns. We interpret the pre-peak as arising from one or more structures containing carbon chains of different lengths. The *c* values of 0.896 and 1.02 nm are only compatible with structures containing C_6 and C_8 chains, respectively. Since grains with the two spacings are platy and elongated, respectively, we conclude that the former contains C_6 chains and the latter C_8 chains. This interpretation is consistent with findings from our synthesis products, in which C_6 chains are more abundant and stable than longer ones[2].

Determination of *a* and *b* are obtained from the positions of the white spots in TEM and STEM images taken both parallel and perpendicular to *c*. Figure 4 illustrates the case for using the images of platy crystals to determine the unit-cell dimensions for the structure containing six-membered carbon chains. Combining the two projections generates a hexagonal unit cell with a gold atom at each corner (orange spheres), and another two at (1/3, 2/3, 1/2) and (2/3, 1/3, 1/2) (yellow spheres) within the cell. A unit cell is indicated with edges highlighted in red and labeled OA, OB, and OC. Measurement gives $a = b = OA = OB = \sim 0.60$ nm and $c = OC = \sim 0.93$ nm, the latter of which matches the PXRD value within the uncertainty of TEM measurements. A similar unit-cell geometry, except that $c = \sim 1.02$ nm, applies to the elongated crystals.

Positions and configurations of carbon chains

Raman and UV absorption spectra indicate the presence of short carbon chains that occur as polyynes. Criteria for placing carbon chains within unit cells are: (1) the number of carbon atoms in a chain, *n*, must be even and likely range from 6 to 16[2]; (2) for stabilization, the carbon chains must exhibit van der Waals interaction with the gold atoms[1] so that the unsaturated triple-bond nature of the carbon chain is sustained; (3) the positions of carbon chains must be compatible with the symmetry of the structure; (4) the carbon chains must be relatively isolated from one another so that cross linking is avoided; and (5) there must be a sufficient number of carbon chains in each unit cell to explain the high concentration of carbon relative to gold.

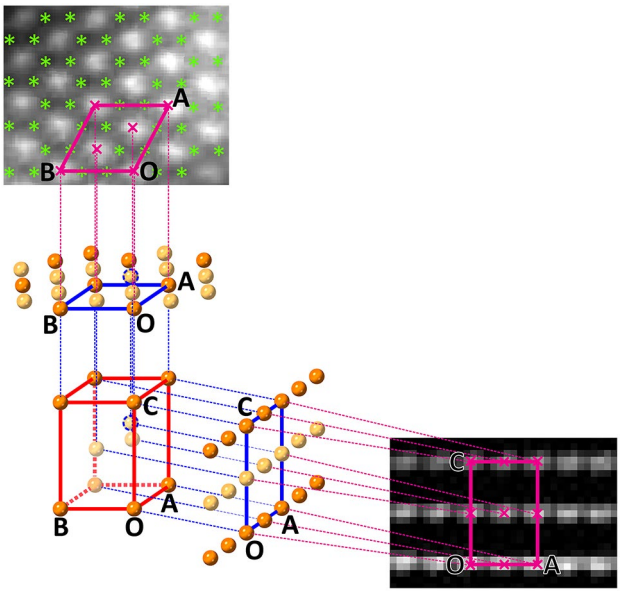

Fig. 4. The unit-cell geometry of platy gold pseudocarbyne, determined from two orthogonal images (top left and bottom right), and positions of the [001] projections of carbon chains (green asterisks). Enlargements, for clarity, of Figs 3c inset and 2d, respectively, are used. The former is from an elongated grain, but its use is justified by the similarity in symmetry and dimensions between its spot pattern and that of a platy crystal (cf. Fig. 2b). The bright spots in each image, some of which are marked by magenta crosses, correspond to the projection of columns and rows, respectively, of gold atoms along [001] and [120]. Atomic radii are reduced for clarity in the "ball-and-stick" model. The yellow sphere marked by a blue dashed circle is from an adjoining unit cell behind the highlighted one.

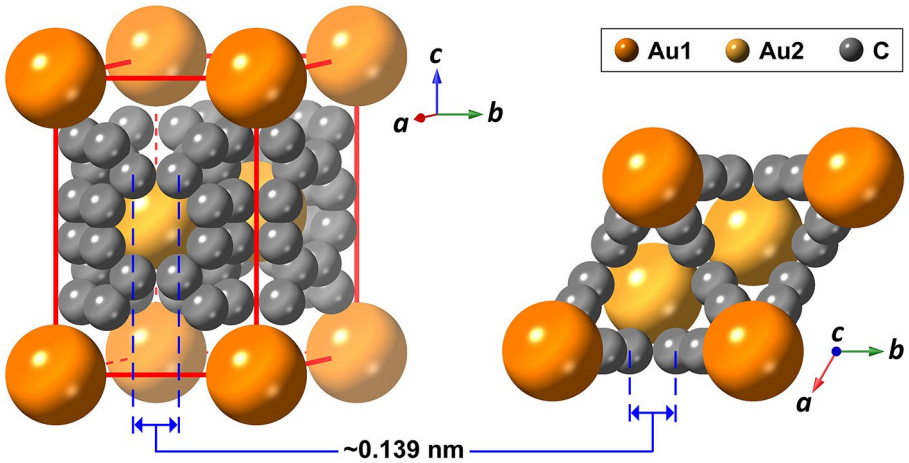

Fig. 5. Structure of platy Au-pseudocarbyne(C_6) viewed along a direction close to [210] and along *c*, as shown in the left and right panel, respectively. The minimum separation of 0.139 nm between adjacent chains is indicated. The relative sizes of the spheres are scaled to the atomic radii of gold and carbon.

The above criteria are satisfied only if the carbon chains are parallel to *c*, with their [001] projections lying along the six equivalent <100> directions and around the sites indicated by green asterisks in Fig. 4. The coordinates of the carbon atoms within a unit cell are then determined by exploring all possibilities using geometrical analysis and then subsequently fitting the PXRD peak intensity ratios (see SI).

Structure model

The proposed structure of Au-pseudocarbyne(C_6) can be visualized as a gold framework enclosing carbon chains (Fig. 5). It differs significantly from those of both gold carbide[35] and copper-capped polyacetylide[36,37]. The unit cell has gold atoms at its corners and at (1/3, 2/3, 1/2) and (2/3, 1/3, 1/2). The carbon chains within the unit cell are oriented parallel to *c* and positioned between any three closest columns of gold atoms as projected along *c*. The

Chemical Formula	AuC_{12}					
Crystal System	Hexagonal					
Space Group	P6/mmm[191]					
Unit-Cell Parameters	$a=b=0.60$ nm, $c=0.896$ nm, $\alpha=\beta=90°$, $\gamma=120°$					
Unit-Cell Volume	0.296 nm^3					
Z	3					
Density	6.083 g/cm^3					
Asymmetric Unit	Au1(0, 0, 0); Au2(0.333, 0.667, 0.500); C1(0.255, 0, 0.227); C2(0.384, 0, 0.329); C3(0.232, 0, 0.433)					
Bond Distance	Au1 – C1	C1 – C2	C2 – C3	C3 – C4	Au2 – C2	Au2 – C3
	0.25(5) nm	0.120 nm	0.130 nm	0.120 nm	0.24(2) nm	0.24(4) nm
Bond Angles	C6 – Au1 – C1	Au1 – C1 – C2	C1 – C2 – C3	C2 – C3 – C4		
	106.(1)°	176.(7)°	95.(4)°	135.(6)°		

Table 1. Structure details of Au-pseudocarbyne with chains containing six carbon atoms. As explained in the SI, the C1-C2, C2-C3, and C3-C4 bond distances are stipulated. The model is compatible with a hydrogen-free structure.

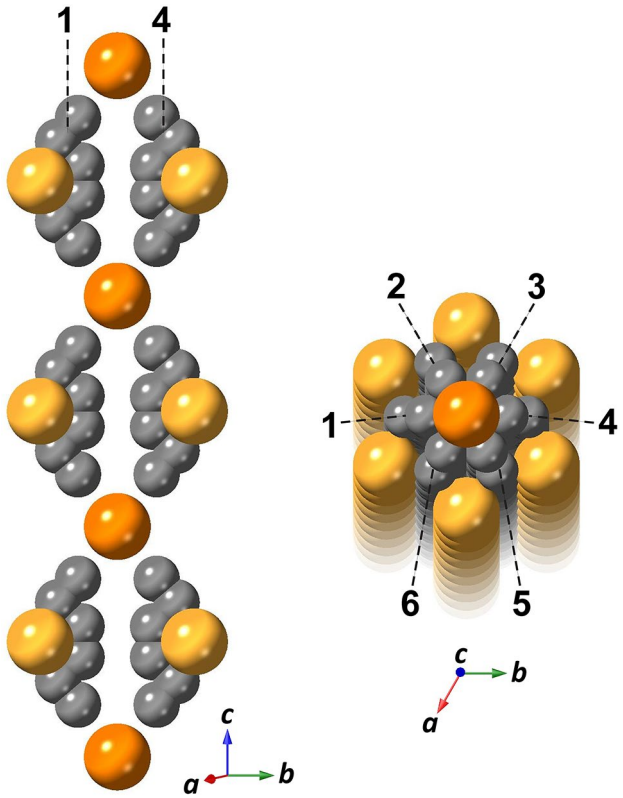

Fig. 6. Extended carbon chains with periodic breaks by the stabilizing gold atoms in Au-pseudocarbyne(C_6). The left panel exhibits two such extended chains, which are numbered 1 and 4, respectively, with associated columns of orange Au1 and yellow Au2 atoms along *c*. The relative positions of these two chains within a "bundle" are shown in the right panel, where the "bundle" can be discerned in a direction close to *c*. The relative size of gold atoms is slightly reduced for improved visibility.

carbon atoms zigzag along the chain lengths. The chains have a gold atom close to each end and are equidistant from two other gold atoms midway along their lengths. The gold-carbon bond lengths at either chain end, *i.e.*, Au1-C1 and Au1-C6, are slightly greater than those near the middle of the chain, *i.e.*, Au2-C2, Au2-C5, Au2-C3, and Au2-C4. Because of the interaction between gold atoms and carbon chains in Au-pseudocarbyne(C_6), the six-membered pseudocarbyne carbon chains are more kinked than those calculated for pure polyynic chains[27]. Details of the optimized structure are given in Table 1.

The chains resulting from the repetition of the unit cell along *c* resemble those proposed for carbyne, except that they zigzag and contain breaks resulting from the stabilizing effects of the gold atoms (Fig. 6, left). They

can be simplified as ···-C≡C-C≡C-C≡C-Au1-C≡C-C≡C-C≡C-··· parallel to *c* and isolated by Au2 atoms from neighboring carbon chains. It is this stabilization that allows the pseudocarbyne structures to avoid cross-linking between the tightly spaced carbon chains. Alternatively, the structure can be understood as parallel "bundles," each consisting of six parallel carbon chains that surround one column of Au1 atoms and are separated from adjacent carbon chains by six columns of Au2 atoms (Fig. 6, right). These "bundles" are intimately intergrown, with a separation of 0.60 nm between adjacent pairs.

The structure model explains the morphology difference between platy and elongated crystals. When n is divisible by four, the two carbon atoms near the middle of a chain are connected by a single bond, and when n is not divisible by four, a triple bond occurs. As a result, more electrons can interact with gold atoms at $z = 1/2$ in the latter cases (*e.g.*, Fig. 5), leading to stronger gold–carbon-chain binding forces and rapid lateral growth of the structure, thereby producing platy crystals. In contrast, the lateral binding forces in crystals with n divisible by four are significantly weaker, promoting growth of nanodomains and elongated crystals.

Carbyne or pseudocarbyne?

Several recent papers from a group in Sun Yat-Sen University (SYSU) describe the synthesis and properties of what they report as carbyne[30,38–42], the carbon allotrope consisting of *sp* carbon only. This work has attracted both attention and questions[1–3,43,44].

Based on the SYSU papers, the reported carbyne samples were synthesized using LAL, just like some of our samples. The SYSU samples display the same PXRD and TEM results, plus similar Raman features as ours, leading to the high probability that both they and we are studying the same materials. However, the SYSU group report that their samples, although synthesized in the presence of gold, are free of gold. In contrast, our samples contain gold as an integral structural component. Additionally, we show the positions of the gold atoms in the crystal structure. Another comparison is that the supposed carbyne samples are described as containing structural features that are shown schematically as kinked. The carbon chains in our three-dimensional crystal structure are also kinked. Furthermore, indexing of their electron diffraction patterns in terms of our structure model can better explain their data. For all the reasons above, we suggest that the SYSU group, like we, has been studying pseudocarbyne rather than carbyne.

Conclusions

The current work reports the crystal structure of Au-pseudocarbyne(C_6) that contains *sp* bonded carbon chains and is stabilized by gold. The carbon chains in the structure lie parallel to its hexagonal axis within a framework of gold atoms. Each chain has six carbon atoms arranged in a kinked configuration. The Au-pseudocarbyne(C_6) crystals have space group P6/mmm[191], with unit-cell parameters $a = b = 0.60$ nm, $c = 0.896$ nm, $\alpha = \beta = 90°$, $\gamma = 120°$. Also, many PXRD patterns and TEM/STEM images indicate d-spacings of ~ 1.02 nm, suggesting the existence of the Au-pseudocarbyne(C_8) structure. Crystals consisting solely of Au-pseudocarbyne(C_6) assume platy shapes, whereas those consisting solely of Au-pseudocarbyne(C_8) are elongated and contain fibrous nanodomains.

Based on the proposed crystal structure, calculations indicate that the electronic structure and spectroscopic properties of the Au-pseudocarbynes resemble those of isolated *sp* carbon chains[1–3,45]. These results suggest that they could be useful for fabricating novel devices based on the predicted properties of carbynes. Another possible application is energy storage owing to the high volume-density of polyynic groups and thus high density of chemical energy. By reference to the data of specific heat of combustion for acetylene, the mass energy density and volume energy density of Au-pseudocarbyne(C_6) are estimated to be on the order of ~ 20 MJ/kg and ~ 130 MJ/L, respectively, while those of Au-pseudocarbyne(C_8) are ~ 25 MJ/kg and ~ 160 MJ/L, respectively. These values are comparable to those of liquid hydrogen, *i.e.*, ~ 10 MJ/kg and ~ 143 MJ/L. Au-pseudocarbyne(C_n) with $n > 8$ would have even higher energy densities.

Data availability

All the research data that support the findings of this study are deposited in the ASU Library Research Data Repository and can be accessed at https://doi.org/10.48349/ASU/3TWEI0. A CIF file corresponding to the opti mized crystal structure of Au-pseudocarbyne(C_6) is also included.

Received: 3 September 2024; Accepted: 18 November 2024
Published online: 02 January 2025

References

1. Tarakeshwar, P., Buseck, P. R. & Kroto, H. W. Pseudocarbynes: Charge-stabilized carbon chains. *J. Phys. Chem. Lett.* **7**, 1675–1681 (2016).
2. Kim, H. et al. Pseudocarbynes: Linear carbon chains stabilized by metal clusters. *J. Phys. Chem. C* **124**, 19355–19361 (2020).
3. Kim, H., Tarakeshwar, P., Meneghetti, M., Buseck, P. R. & Sayres, S. G. Formation of Au-pseudocarbynes by self-assembly of carbon chains and gold clusters. *Carbon* **205**, 546–551 (2023).
4. Banhart, F. Chains of carbon atoms: A vision or a new nanomaterial?. *Beilstein J. Nanotechnol.* **6**, 559–569 (2015).
5. Casari, C. S., Tommasini, M., Tykwinski, R. R. & Milani, A. Carbon-atom wires: 1-D systems with tunable properties. *Nanoscale* **8**, 4414–4435 (2016).
6. Bryce, M. R. A review of functional linear carbon chains (oligoynes, polyynes, cumulenes) and their applications as molecular wires in molecular electronics and optoelectronics. *J. Mater. Chem. C* **9**, 10524 (2021).
7. Yang, G. Synthesis, properties, and applications of carbyne nanocrystals. *Mater. Sci. Eng. R Rep.* **151**, 100692 (2022).
8. Jin, C., Lan, H., Peng, L., Suenaga, K. & Iijima, S. Deriving carbon atomic chains from graphene. *Phys. Rev. Lett.* **102**, 205501 (2009).
9. Shi, L. et al. Confined linear carbon chains as a route to bulk carbyne. *Nat. Mater.* **15**, 634–639 (2016).

10. Kudryavtsev, Y. P., Evsyukov, S. E., Guseva, M. B., Babaev, V. G. & Khvostov, V. V. Carbyne: The third allotropic form of carbon. *Russ. Chem. B* **42**, 399–413 (1993).
11. Kavan, L. & Kastner, J. Carbyne forms of carbon: Continuation of the story. *Carbon* **32**, 1533–1548 (1994).
12. Kastner, J., Kuzmany, H., Kavan, L., Dousek, F. P. & Kürti, J. Reductive preparation of carbyne with high yield. An in-situ Raman scattering study. *Macromolecules* **28**, 344–353 (1995).
13. Heimann, R. B. In *Carbyne and Carbynoid Structures* (eds Heimann, R. B. et al.) 7–15 (Kluwer, 1999).
14. Kudryavtsev, Y. P. In *Carbyne and Carbynoid Structures* (eds Heimann, R. B. et al.) 1–6 (Kluwer, 1999).
15. Li, S.-Y., Zhou, H.-H., Gu, J.-L. & Zhu, J. Does carbyne really exist? Carbynes in expanded graphite. *Carbon* **38**, 929–941 (2000).
16. Chuan, X. Y., Wang, T. K. & Donnet, J.-B. Stability and existence of carbyne with carbon chains. *New Carbon Mater.* **20**, 83–91 (2005).
17. Korobova, J. G., Guseva, M. B., Bazhanov, D. I. & Khvostov, V. V. In *Carbon Nanomaterials in Clean Energy Hydrogen Systems-II* (eds Zaginaichenko, S. Y. et al.) 469–485 (Springer, 2011).
18. Baughman, R. H. Dangerously seeking linear carbon. *Science* **312**, 1009–1010 (2006).
19. Kroto, H. W. Carbyne and other myths about carbon. *Chem. World* **7**, 37 (2010).
20. Tykwinski, R. R. et al. Toward carbyne: Synthesis and stability of really long polyynes. *Pure Appl. Chem.* **82**, 891–904 (2010).
21. Arora, A. et al. Monodisperse molecular models for the *sp* carbon allotrope carbyne; Syntheses, structures, and properties of diplatinum polyynediyl complexes with $PtC_{20}Pt$ to $PtC_{52}Pt$ linkages. *ACS Cent. Sci.* **9**, 2225–2240 (2023).
22. Whittaker, A. G. & Watts, E. J. Carbynes: Carriers of primordial noble gases in meteorites. *Science* **209**, 1512–1514 (1980).
23. Whittaker, A. G. Carbyne forms of carbon: Evidence for their existence. *Science* **229**, 485–486 (1985).
24. Lumpkin, G. R. Electron microscopy of carbon in Allende acid residues. *Lunar Planet. Sci.* **12**, 631 (1981).
25. Smith, P. P. K. & Buseck, P. R. Carbyne forms of carbon: Do they exist?. *Science* **216**, 984–986 (1982).
26. Smith, P. P. K. & Buseck, P. R. Reply to carbyne forms of carbon: Do they exist?. *Science* **229**, 486–487 (1985).
27. Heimann, R. B., Kleiman, J. & Salansky, N. M. A unified structural approach to linear carbon polytypes. *Nature* **306**, 164–167 (1983).
28. Korshak, V. V., Kasatochkin, V. I., Kudriavt, I. P., Usenbaev, K. & Sladov, A. M. Synthesis and properties of polyacetylene. *Dokl. Akad. Nauk SSSR* **136**, 1342 (1961).
29. Kasatochkin, V. I., Melnichenko, V. M. & Elizen, V. M. Electron diffraction by single crystals of carbyne. *Polym. Sci.* **17**, 2167–2173 (1975).
30. Pan, B. et al. Carbyne with finite length: The one-dimensional *sp* carbon. *Sci. Adv.* **1**, e1500857 (2015).
31. Weisbach, N. et al. Triisopropylsilyl (TIPS) alkynes as building blocks for syntheses of platinum triisopropylsilylpolyynyl and diplatinum polyynediyl complexes. *Organometallics* **38**, 3294–3310 (2019).
32. Salazar, J. J. V. et al. Fabrication of carbon chains (pseudo carbynes) by stabilization with gold-thiol complex. *Carbon* **225**, 119118 (2024).
33. Wang, J. et al. Tuning point defects by elastic strain modulates nanoparticle exsolution on perovskite oxides. *Chem. Mater.* **33**, 5021–5034 (2021).
34. Jolly, A. & Benilan, Y. Review of quantitative spectroscopy of polyynes. *J. Quant. Spectrosc. Radiat. Transf.* **109**, 963–973 (2008).
35. Westenfelder, B. et al. Bottom-up formation of robust gold carbide. *Sci. Rep.* **5**, 8891 (2015).
36. Cataldo, F. A study on the structure and electrical properties of the fourth carbon allotrope: Carbyne. *Polym. Int.* **44**, 191–200 (1997).
37. Cataldo, F. From dicopper acetylide to carbyne. *Polym. Int.* **48**, 15–22 (1999).
38. Chen, T., Yang, F., Wu, X., Chen, Y. & Yang, G. A fluorescent and colorimetric probe of carbyne nanocrystals coated Au nanoparticles for selective and sensitive detection of ferrous ions. *Carbon* **167**, 196–201 (2020).
39. Yang, F., Li, C., Li, J., Liu, P. & Yang, G. Carbyne nanocrystal: one-dimensional van der Waals crystal. *ACS Nano* **15**, 16769–16776 (2021).
40. Yang, F., Zheng, Z., He, Y., Liu, P. & Yang, G. A new wide bandgap semiconductor: carbyne nanocrystals. *Adv. Funct. Mater.* **31**, 2104254 (2021).
41. Yang, G. Synthesis, properties, and applications of carbyne nanocrystals. *Mater. Sci. Eng. R* **151**, 100692 (2022).
42. Cao, W., Xu, H., Liu, P., He, Y. & Yang, G. The kinked structure and interchain van der Waals interaction of carbyne nanocrystals. *Chem. Sci.* **14**, 338–344 (2023).
43. Davenport, M. Contention over carbyne. *Chemical & Engineering News*. https://cen.acs.org/articles/93/i46/Contention-Over-Carbyne.html (2015).
44. Lowe, D. New forms of carbon? *Science Commentary*. https://www.science.org/content/blog-post/new-forms-carbon (2015).
45. Tarakeshwar, P., Buseck, P. R. & Timmes, F. X. On the structure, magnetic properties, and infrared spectra of iron pseudocarbynes in the interstellar medium. *Astrophys. J.* **879**, 2 (2019).

Acknowledgements

This research was financially supported by the W. M. Keck Foundation and Arizona State University. We gratefully acknowledge the use of facilities within the Eyring Materials Center at Arizona State University. We also thank Shize Yang at ASU for technical assistance in acquisition of the STEM-EELS data. Miguel J. Yacaman and Blake Rogers are acknowledged for discussions about their thiolate-stabilized pseudocarbyne.

Author contributions

J.W. acquired and analyzed the TEM data and modelled the structure. J.W. and P.R.B. wrote the manuscript, with contributions from all co-authors. P.R.B. and P.T. conceived the concept of the project. H.K., S.G.S. and M.M. prepared the samples and analyzed the spectroscopic data. J.B. acquired some of the TEM data.

Competing interests

The authors declare no competing interests.

Additional information

Supplementary Information The online version contains supplementary material available at https://doi.org/10.1038/s41598-024-80359-5.

Correspondence and requests for materials should be addressed to J.W. or P.R.B.